Intracluster Reaction, Fragmentation, and Structure of Monomethylamine, Dimethylamine, and Trimethylamine Cluster Ions

ARTICLE *in* THE JOURNAL OF PHYSICAL CHEMISTRY · SEPTEMBER 1996

Impact Factor: 2.78 · DOI: 10.1021/jp961303b

Intracluster Reaction, Fragmentation, and Structure of Monomethylamine, Dimethylamine, and Trimethylamine Cluster Ions

W. B. Tzeng,* K. Narayanan, and G. C. Chang

Institute of Atomic and Molecular Sciences, Academia Sinica, P.O. Box 23-166, Taipei 106, Taiwan, Republic of China

W. C. Tsai and J. J. Ho

Department of Chemistry, National Taiwan Normal University, 88 Sec. 4, Tingchow Road, Taipei 117, Taiwan, Republic of China

Received: May 7, 1996; In Final Form: June 21, 1996[⊗]

Ammonia, monomethylamine (MMA), dimethylamine (DMA), and trimethylamine (TMA) clusters, formed in a supersonic expansion, were investigated using a multiphoton ionization time-of-flight mass spectrometer. The observed major product ions resulting from prompt fragmentation following ionization are $(NH_3)_nH^+$, $(CH_3NH_2)_nH^+$, $[(CH_3)_2NH]_nH^+$, and $[(CH_3)_3N]_nH^+$. Detection of stable $CH_2{=}NH_2^+$ and $(CH_2{=}NH{-}CH_3)^+$ immonium ions and other fragments provides evidence for molecular rearrangement and fragmentation within our observable time windows. Anomalously large relative intensities observed for $(NH_3)_5H^+$, $(CH_3NH_2)_4H^+$, $[(CH_3)_2NH]_3H^+$, and $[(CH_3)_3N]_2H^+$ are attributed to enhanced stability of the cluster ions, due to the complete filling of hydrogen-bonding sites on the "central ions". Fully optimized geometries and stabilization energies of these cluster ions have been predicted using *ab initio* molecular orbital methods. The experimental findings are in very good agreement with the calculated results.

1. Introduction

Investigations of cluster ions in the gas phase provide important information about physicochemical properties, such as intermolecular interaction between solvent molecules with the ion. It is known that hydrogen bonding plays a significant role in the transition from the molecular level to the complex macroscopic level, as in the case of cluster systems. Theoretical[1,2] and experimental[3−5] studies on $(H_2O)_nH^+$ and $(NH_3)_nH^+$ clusters suggest a central ion core structure for these species. In particular, $(H_2O)_4H^+$ and $(NH_3)_5H^+$ exhibit extra stability due to the formation of complete solvation shells. The central ions H_3O^+ and NH_4^+ provide a maximum of three and four hydrogen-bonding sites for the surrounding molecules. Cluster ion abundance reflects the stability of the ionic species but does not necessarily correlate with the relative stability of the neutral species.[6,7]

Ammonia cluster ions have been extensively studied by various researchers and the existence of magic numbers for a particular cluster size is very well established.[8,9] MMA, DMA, and TMA clusters up to pentamers have been studied by photoionization mass spectrometry from which absolute proton affinities, proton solvation energies, and intermolecular bond energies were deduced from the measured ionization and appearance energies.[10−12] However, to the best of our knowledge, no investigation has been reported in the case of methylated amine cluster ions. The main objective of this study is therefore to investigate whether these cluster ion sequences exhibit magic numbers due to enhanced stability for a particular cluster size. In addition, the intracluster reaction, fragmentation, and stable structure for amine clusters in the gas phase are also investigated.

The experimental work involves the use of time-of-flight mass spectrometry (TOFMS) in conjunction with multiphoton ionization (MPI) to investigate protonated MMA, DMA, and TMA clusters. Fully optimized geometric structures and total energies for these cluster ions were computed using *ab initio* molecular orbital (MO) methods with basis sets containing both polarization and diffusion functions. Based on calculated values, the stabilization energies $\Delta E_{n-1,n}$ of these cluster ions have been deduced and compared with the available experimental values.

2. Experimental and Computational Details

2.1. Experimental Section. The experiments were performed with a laser-based photoionization TOF mass spectrometer as described in our earlier publications.[13,14] Briefly, the neutral ammonia, MMA, DMA, and TMA clusters were produced in a supersonic expansion by seeding about 0.3 bar of the corresponding gas sample in helium at a total pressure of 3 bar. The pulsed valve was operated at 10 Hz with a pulse duration of 300 μs. The cluster beam was collimated by a skimmer located 15 mm downstream from the nozzle orifice (30° cone angle, 0.15 mm diameter). Typical operational pressures in the gas expansion and the ionization chambers were 7×10^{-3} and 8×10^{-6} Pa, respectively.

The ionization wavelength was the third harmonic (355 nm) from a Quanta Ray GCR-3 Nd-YAG laser. A delay of 800 μs was applied to the ionization laser with respect to the pulsed valve. The laser light was then focused perpendicularly to the molecular beam about 50 mm from the nozzle orifice. The ions generated as a result of MPI were accelerated to about 2 keV into the field-free region toward a Chevron microchannel plate (MCP) detector. The TOF ion signals from the MCP were recorded with a Stanford Research Systems SR430 multichannel scaler (MCS). All TOF mass spectra reported in this paper were accumulated for 600 laser shots.

* Corresponding author. Address for correspondence: Dr. Wen-Bih Tzeng, Institute of Atomic and Molecular Sciences, Academia Sinica, P.O. Box 23-166, #1 Section 4, Roosevelt Road, Taipei 106, Taiwan, R.O.C. Phone: (886)2-366-8236. Fax: (886)2-362-0200. E-mail: wbt@po.iams.sinica.edu.tw.

⊗ Abstract published in *Advance ACS Abstracts,* August 15, 1996.

S0022-3654(96)01303-2 CCC: $12.00

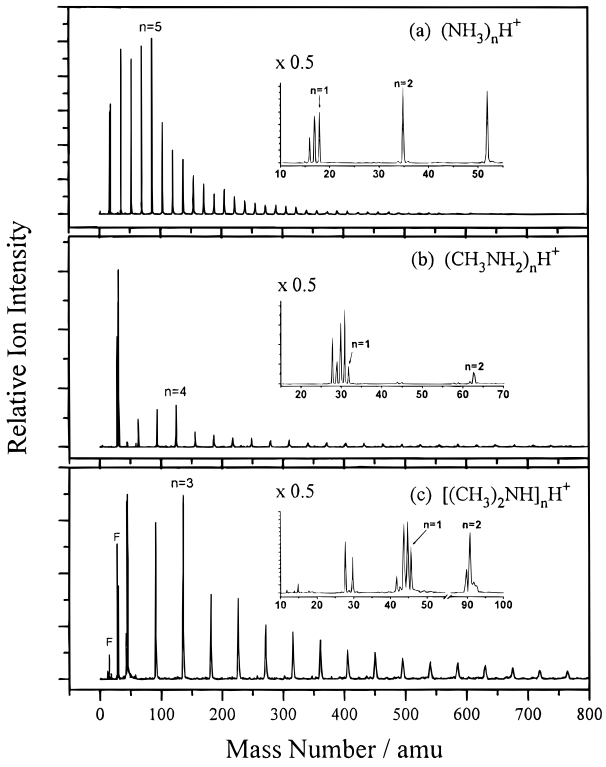

Figure 1. TOF mass spectra of photoionized ammonia, MMA, and DMA clusters recorded at a laser wavelength of 355 nm. The observed cluster ions are (a) $(NH_3)_nH^+$ ($n = 1-32$), (b) $(CH_3NH_2)_nH^+$ ($n = 1-24$), and (c) $[(CH_3)_2NH]_nH^+$ ($n = 1-17$). Labels on each of the nearly equally-spaced peaks designate the number of corresponding molecules in the cluster ions.

Anhydrous ammonia obtained from Air Products was 99.99% pure. MMA, DMA, and TMA (Matheson Gas Products) had a nominal purity of 99.99%. All chemicals were used without further purification.

2.2. Computational Section. *Ab initio* MO calculations were carried out on a IBM RS6000 590 work station using the GAUSSIAN 94 program package.[15] No geometric constraints were imposed to obtain the fully optimized cluster and molecular geometries. The Hartree−Fock (HF) procedure was performed for all the systems using the 3-21G, 6-31G*, 6-31G**, and 6-31+G* basis sets while second order Møller−Plesset (MP2) perturbation computations were performed on selective systems using 6-31G*, 6-31G**, 6-31+G*, and 6-31+G** basis sets. Calculations with the above given basis sets are found to reproduce the pyramidal structure of ammonia with the ∠HNH angle in very good agreement with the experimentally determined value of 106.7°. The 4-31G and 6-31G basis sets were not used as calculations using these basis sets overestimated the ∠HNH resulting in an almost planar optimized geometry. For large cluster ion systems involving many ligands, calculations with higher basis sets were limited with our present computational facilities.

3. Results

3.1. TOF Mass Spectra of Photoionized Ammonia, MMA, DMA, and TMA Clusters. The TOF mass spectra of photoionized ammonia, MMA and DMA clusters recorded at a laser wavelength of 355 nm are shown in Figure 1. The observed major protonated cluster ions are (a) $(NH_3)_nH^+$ ($n = 1-32$), (b) $(CH_3NH_2)_nH^+$ ($n = 1-24$), and (c) $((CH_3)_2NH)_nH^+$ ($n = 1-17$). Anomalously large signals appear at $n = 5$, 4, and 3 in the relative intensity distributions of $(NH_3)_nH^+$, $(CH_3NH_2)_nH^+$, and $((CH_3)_2NH)_nH^+$, respectively. Dependence of laser fluence on the signal intensities revealed that the ionization processes

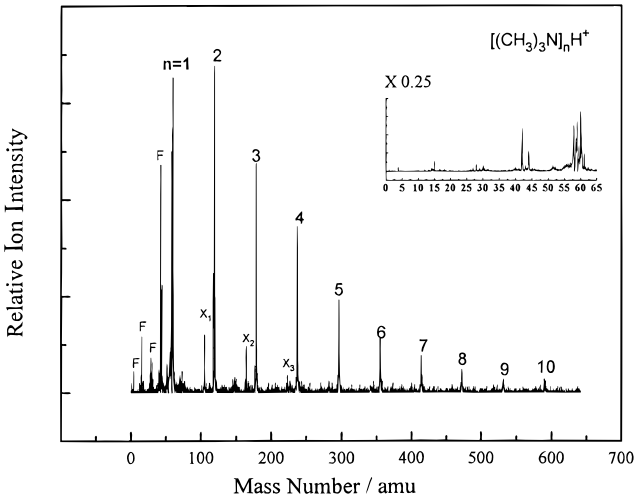

Figure 2. TOF mass spectrum of photoionized TMA clusters. Major cluster ions are $[(CH_3)_3NH]_nH^+$ ($n = 1-10$). Labels on each of nearly equally-spaced peaks designate the number of $(CH_3)_3N$ molecules in the cluster ions. $X_m \equiv [(CH_3)_3N]_m[(CH_3)_2NH]H^+$ ($m = 1-3$); F ≡ fragment ions.

involve three photons in the laser power range 0.03−0.15 W.[14] To ensure that the observed features are not due to experiential artifacts, we have surveyed various conditions such as, gaseous sample composition, stagnation pressure behind the pulse valve, laser power, and the time delay between the cluster beam and the ionization laser. All these results, however, yield the spectral features mentioned above.

As evident from Figure 1a, the major product ions resulting from the photoionization of ammonia clusters are NH_2^+, $NH_3^{\bullet+}$, and $(NH_3)_nH^+$ generated from prompt intracluster reaction and fragmentation.[5] For MMA clusters, spectral peaks at masses 28, 29, 30, 44, 45, 58, and 59 were observed in addition to the protonated and unprotonated peaks as shown in Figure 1b. Analysis of the spectral features revealed that the peak at masses 28 and 29 correspond to the $CH{\equiv}NH^+$ and $CH_2{=}NH^{\bullet+}$. The peaks at masses 30 and 44 provide evidence for the formation of stable immonium ions $CH_2{=}NH_2^+$ and $(CH_2{=}NH{-}CH_3)^+$. The relatively weak features at masses 45, 58, and 59 are found to be due to $(CH_2{-}NH_2{-}CH_3)^{\bullet+}$, $[(CH_2{=}NH)\cdot(NH{=}CH_2)]^{\bullet+}$, and $[(CH_2{=}NH)\cdot(NH_2{=}CH_2)]^+$, resulting from intracluster rearrangement and fragmentation of the protonated MMA clusters.

In the case of DMA clusters, in addition to the characteristic peaks corresponding to protonated and unprotonated species, peaks at masses 15, 28, 30, 42, and 44 were observed. The TOF peaks are found to be broader for larger cluster ions which may result from metastable processes. Clearly, those peaks at masses 30 and 44 are due to the immonium ions $CH_2{=}NH_2^+$ and $(CH_2{=}NH{-}CH_3)^+$. The peak corresponding to mass 42 is an indication of fragment ions in the form of $(CH_3{-}N{\equiv}CH)^+$.[16] The peak at mass 28 is assigned to $CH{\equiv}NH^+$ while that at mass 15 to NH^+ or CH_3^+.

The TOF mass spectrum of the photoionized TMA clusters at 355 nm is shown in Figure 2. The results show that the observed major cluster ions are $[(CH_3)_3N]_nH^+$ with an intensity maximum at $n = 2$. Less intense peaks due to the unprotonated species $[(CH_3)_3N]_n^{\bullet+}$ are also observed. The spectral peaks at masses 105, 164, and 223 are due to the heterocluster ions $[(CH_3)_3N]_n\cdot[(CH_3)_2NH]H^+$ ($n = 1-3$) which result from the trace amounts of DMA present in the gas inlet lines.

The spectral peaks at masses 58, 59, and 60 are assigned to $[(CH_3)_2N{=}CH_2]^+$, $(CH_3)_3N^{\bullet+}$ and $[(CH_3)_3NH]^+$, respectively while those at masses 42 and 44 result from $(CH_3{-}N{\equiv}CH)^+$ and $(CH_2{=}NH{-}CH_3)^+$ cluster ions. Satellite peaks at masses

TABLE 1: Total Energies[a] of Radical Cation Species (A) $(CH_3NH_2CH_2)^{\bullet+}$, (B) $(CH_3NHCH_3)^{\bullet+}$, and Cation Species (C) $(CH_3NCH)^+$, and (D) $(CH_2NCH_2)^+$

calculation	*E* (hartrees) (A)	*E* (hartrees) (B)	ΔE (A − B) (kJ/mol)	*E* (hartrees) (C)	*E* (hartrees) (D)	ΔE (C − D) (kJ/mol)
HF/6-31G*	−133.972 29	−133.985 38	−34.3	−132.221 98	−132.214 38	−20.0
HF/6-31G**	−133.987 68	−133.998 90	−29.5	−132.229 12	−132.221 69	−19.5
HF/6-31+G*	−133.973 37	−133.986 10	−33.4	−132.222 86	−132.215 84	−18.4
MP2/6-31G*	−134.763 22	−134.763 62	−1.1	−133.033 44	−133.005 82	−72.5
MP2/6-31G**	−134.858 14	−134.857 78	+0.9	−133.084 18	−133.056 75	−72.0
MP2/6-31+G**	−134.863 14	−134.862 13	+2.7	−133.087 95	−133.061 28	−70.0

[a] 1 hartree = 2625.5 kJ/mol.

TABLE 2: Total Energy[a] (*E*) and Stabilization Energies ($\Delta E_{n-1,n}$) of Ammonia and Its Cluster Ions

species	*E* (hartrees) HF/3-21G	HF/6-31G**	HF/6-31+G*	MP2/6-31G*	$\Delta E_{n-1,n}$ (kJ/mol) HF/3-21G	HF/6-31G**	HF/6-31+G*	MP2/6-31G*	$\Delta H_{n-1,n}$ (kJ/mol)
NH_3	−55.872 20	−56.195 54	−56.189 50	−56.524 60					
NH_4^+	−56.233 86	−56.545 53	−56.531 28	−56.870 62	−949.5	−918.9	−897.3	−908.5	−853.5 [19]
$(NH_3)_2H^+$	−112.165 21	−112.782 84	−112.758 94	−113.453 68	−155.3	−109.7	−100.2	−153.5	−106.3 [28]
$(NH_3)_3H^+$	−168.080 01	−169.011 27	−168.979 05	−170.020 66	−111.8	−86.4	−80.4	−111.3	−72.4 [28]
$(NH_3)_4H^+$	−223.986 44	−225.233 92	−225.193 99		−89.9	−71.2	−66.8		−59.4 [28]
$(NH_3)_5H^+$	−279.886 52	−281.452 09	−281.404 93		−73.2	−59.4	−56.3		−49.4 [28]
$(NH_3)_6H^+$	−335.778 06	−337.660 27	−337.605 72		−50.8	−33.2	−29.6		−29.3 [28]
$(NH_3)_7H^+$	−391.668 79				−48.7				−25.1 [5]

[a] 1 hartree = 2625.5 kJ/mol.

TABLE 3: Total Energy[a] (*E*) and Stabilization Energies ($\Delta E_{n-1,n}$) of MMA, DMA, TMA, and Their Cluster Ions

species	*E* (hartrees) HF/3-21G	HF/6-31G**	HF/6-31+G*	MP2/6-31G*	$\Delta E_{n-1,n}$ (kJ/mol) HF/3-21G	HF/6-31G**	HF/6-31+G*	MP2/6-31G*	$\Delta H_{n-1,n}$ (kJ/mol)
MMA	−94.681 66	−95.221 86	−95.214 17	−95.803 97					
$(MMA)H^+$	−95.059 34	−95.588 87	−95.574 16	−96.163 86	−991.6	−963.6	−945.2	−944.9	−896 [19]
$(MMA)_2H^+$	−189.793 61	−190.847 80	−190.822 53	−192.025 00	−138.1	−97.5	−89.8	−150.1	−89.5 [28]
$(MMA)_3H^+$	−284.513 62	−286.099 01	−286.064 15		−100.7	−77.1	−72.0		
$(MMA)_4H^+$	−379.226 17	−381.345 03	−381.300 92		−81.1	−63.4	−59.3		
$(MMA)_5H^+$	−473.921 37				−35.5				
DMA	−133.494 85	−134.251 75	−134.242 64	−135.092 67					
$(DMA)H^+$	−133.882 95	−134.629 96	−134.614 27	−135.460 88	−1019.0	−993.0	−975.7	−966.7	−923 [19]
$(DMA)_2H^+$	−267.424 60	−268.914 07	−268.886 79		−122.9	−85.0	−78.4		−86.2 [28]
$(DMA)_3H^+$	−400.954 20	−403.191 69	−403.153 52		−91.2	−67.9	−63.2		
TMA	−172.310 27	−173.282 99	−173.272 91	−174.388 98					
$(TMA)H^+$	−172.705 53	−173.668 68	−173.651 61	−174.761 48	−1037.8	−1012.6	−994.1	−978.0	−942 [19]
$(TMA)_2H^+$	−345.057 79	−346.979 79	−346.950 29		−110.2	−73.8	−67.8		−72.4 [28]
$(TMA)_3H^+$	−517.383 97				−41.8				

[a] 1 hartree = 2625.5 kJ/mol.

14, 26, 27, 28, and 29 are assigned to N^+, $C{\equiv}N^{\bullet+}$, $CH{\equiv}N^+$, $CH{\equiv}NH^+$, $CH_2{=}N^{\bullet+}$, and fragment hydrocarbon ions.

3.2. *Ab Initio* Calculations. Table 1 lists the total energies of the fragment species $(CH_3{-}NH_2{-}CH_2)^{\bullet+}$, $(CH_3{-}NH{-}CH_3)^{\bullet+}$, and $(CH_3{-}N{\equiv}CH)^+$, $(CH_2{=}N{=}CH_2)^+$ at various levels of calculation in order to clarify their relative stability. The stabilization energies $\Delta E_{n-1,n}$ calculated using HF and MP2 methods with various basis sets for the $(NH_3)_nH^+$, $(CH_3NH_2)_nH^+$, $[(CH_3)_2NH]_nH^+$, and $[(CH_3)_3N]_nH^+$ cluster ions are displayed in Tables 2 and 3. The trend of these values, as a function of the cluster size, agrees well with the experimentally measured cluster ion intensity distributions.

4. Discussion

4.1. Intracluster Reactions. For convenience of discussion, we use RR′R″N as a general formula for the following compounds: ammonia (R = R′ = R″ = H), MMA (R = CH_3; R′ = R″ = H), DMA (R = R′ = CH_3; R″ = H), and TMA (R = R′ = R″ = CH_3). The first step in the photoionization process of a neutral cluster $(RR'R''N)_p$ can be represented as

$$(RR'R''N)_p + nh\nu \rightarrow (RR'R''N)_p{}^{+}{}^{*} + e^- \qquad (1)$$

where *n* is number of photons involved in the ionization process. The excess energy upon ionization is partitioned into the kinetic energy of the ejected electron and the internal energy of the ionic species $(RR'R''N)_p{}^{+}{}^{*}$. The internally excited $(RR'R''N)_p{}^{+}{}^{*}$ can then rearrange to a more stable structure, or alternatively fragment into other ionic species.

Studies of ammonia cluster ions using two-color two-photon ionization have shown that two intracluster reaction mechanisms occur for clusters of different sizes.[17] The NH_4^+ is produced by spontaneous dissociation of $(NH_3)_2{}^+$ following two-photon ionization of $(NH_3)_2$, whereas $(NH_3)_nH^+$ ($n = 2{-}5$) are formed by ionization of $(NH_3)_nH$ radicals, produced following dissociation of electronically excited neutral ammonia clusters, through a nonresonant three-photon ionization process. Recall that the major product ions of the photoionized ammonia, MMA, and DMA clusters are $(NH3)_nH^+$, $(CH_3NH_2)_nH^+$, and $[(CH_3)_2NH]_nH^+$. As shown in Figure 1, the signals from the unprotonated cluster ions are considerably weaker than those of the corresponding protonated species, except in the case of the monomers. These results are similar to electron impact ionization experiments using an electron energy of 21 eV as well as photoionization experiments using synchrotron radiation with a photon energy of 20.65 eV.[10] It is obvious from these results that large excess energy upon ionization leads to intracluster ion−molecule reactions in $(RR'NH)_p{}^{+}{}^{*}$.

It is known that hydrogen-bonded clusters will fragment upon ionization via proton-transfer reactions. In order to investigate the feasibility of the intracluster proton-transfer reaction in $(RR'NH)_p^{+}$*, we first consider the following analogous bimolecular ion−molecule reactions: (a) $NH_3^+ + NH_3$, (b) $CH_3NH_2^+ + CH_3NH_2$, and (c) $[CH_3]_2NH^+ + [CH_3]_2NH$. With the known ionization potentials,[18] proton affinities,[19] and bond dissociation energies,[20] the estimated enthalpies of possible proton (or hydrogen) transfer reactions are

$$NH_3^+ + NH_3 \rightarrow NH_4^+ + NH_2 \qquad \Delta H = -71.4 \text{ kJ/mol} \quad (2)$$

$$CH_3NH_2^+ + CH_3NH_2 \rightarrow CH_3NH_3^+ + CH_3NH \qquad \Delta H = -30.9 \text{ kJ/mol} \quad (3)$$

$$(CH_3)_2NH^+ + (CH_3)_2NH \rightarrow (CH_3)_2NH_2^+ + (CH_3)_2N \qquad \Delta H = -22.2 \text{ kJ/mol} \quad (4)$$

Therefore, the analogous intracluster reaction in $(RR'NH)_p^{+}$* is expected to proceed spontaneously. In general, this reaction may be expressed as

$$(RR'NH)_p^{+}* \equiv \{[(RR'NH)_{p-2}]\cdot[(RR'NH)^+\cdot\cdot(RR'NH)]\}* \xrightarrow{H^+ \text{ (or H) transfer}} \{[(RR'NH)_{p-2}]\cdot[(RR'NH)H^+\cdot\cdot(RR'N)]\}* \xrightarrow{\text{fragmentation}} [(RR'NH)_{p-1-x}]H^+ + RR'N + xRR'NH \quad (5)$$

Most of the excess energy in this process will be taken away by the neutral fragment products.

The measurement of the lowest appearance potentials of protonated clusters $(RR'NH)_nH^+$ ($n = p - 1 - x$) using a near-threshold photoionization method[10,11] corresponds to the case of $x = 0$ in process 5. The second onset in the photoionization efficiency (PIE) curves of $(CH_3NH_2)_nH^+$ ($n = 1-3$) and $[(CH_3)_2NH]_nH^+$ ($n = 1-3$) have been measured to be in the range of 8.0−8.8 eV which are slightly higher than the lowest appearance potentials of the corresponding species. These values were interpreted as the thresholds for the fragmentation process (5) in the case of $x \geq 1$. For a nonresonant three-photon ionization process at 355 nm, the total photon energy is about 10.5 eV, which is much higher than the second appearance energies of the observed protonated MMA and DMA clusters. Thus, the intracluster reactions in the excited species $(CH_3NH_2)_p^{+}$* and $[(CH_3)_2NH]_p^{+}$* are expected to undergo process 5 with $x \geq 1$.

Photoionization of TMA clusters were performed under similar experimental conditions but, with a higher mass resolution. As shown in Figure 2, the major product cluster ions are $[(CH_3)_3N]_nH^+$ ($n = 1-10$). Since there is no hydrogen atom bound to the nitrogen atom in the TMA molecule, the only possible bonding in the excited species $[(CH_3)_3N]_p^{+}$* is the weak bond of the type N···H−C. The observation of the intense signals corresponding to the $[(CH_3)_3N]_nH^+$ indicates the occurrence of the following intracluster reaction:

$$[(CH_3)_3N]_p^{+}* \equiv \{[(CH_3)_3N]_{p-2}\}\cdots[(CH_3)_3N\cdot\cdot H\cdot\cdot CH_2N(CH_3)_2]^{+}* \xrightarrow{\text{fragmentation}} [(CH_3)_3N]_{p-1-x}H^+ + (CH_3)_2N\,CH_2 + x(CH_3)_3N \quad (6)$$

The product ions $[(CH_3)_3N]_n^{\bullet+}$ are formed through the following simple fragmentation process:

$$[(CH_3)_3N]_p^{+}* \xrightarrow{\text{fragmentation}} [(CH_3)_3N]_n^{\bullet+} + (p-n)(CH_3)_3N \quad (7)$$

4.2. Rearrangement and Fragmentation. 4.2.1. MMA Cluster Ions. It is possible that the product cluster ions may undergo rearrangement and fragmentation within our detection time windows (a few microseconds). For instance, the peak at mass 30 in Figure 1b is assigned to $CH_2{=}NH_2^+$ ion. This is a direct evidence for the 1,2-hydrogen elimination in the protonated MMA. The $CH_2{=}NH_2^+$ ion may lose a hydrogen atom to form the $CH_2{=}NH^{\bullet+}$ (mass 29) or proceed with another 1,2-hydrogen elimination to form the $CH{\equiv}NH^+$ ion (mass 28). In a similar fashion, the protonated MMA dimer is expected to undergo a 1,2-hydrogen elimination to form $[(CH_3NH_2)\cdot(NH_2{=}CH_2)]^+$ (mass 61). Nevertheless, absence of the peak at mass 61 suggests that the $(CH_3NH_2)_2H^+$ undergoes two sequential steps of 1,2-hydrogen elimination to form the $[(CH_2{=}NH_2)\cdot(NH{=}CH_2)]^+$ ion (mass 59). This species can further lose a hydrogen atom to yield $[(CH_2{=}NH)\cdot(NH{=}CH_2)]^{\bullet+}$ (mass 58).

As shown in Figure 3, the protonated MMA dimer may proceed with an intracluster rearrangement, losing a NH_3 molecule to form an intermediate species $(CH_3{-}NH_2{-}CH_3)^+$. This ion, which is similar to the protonated DMA, may undergo the 1,2-hydrogen elimination to form the immonium ion $(CH_2{=}NH{-}CH_3)^+$ (mass 44). Alternatively, it may lose only one hydrogen atom yielding a radical species (mass 45) of the form $(CH_3{-}NH_2{-}CH_2)^{\bullet+}$ or $(CH_3{-}NH{-}CH_3)^{\bullet+}$. The calculated C−N and N−C bond lengths in the $(CH_3{-}NH_2{-}CH_2)^{\bullet+}$ are 1.517 and 1.463 Å, indicating an occurrence of asymmetric charge distribution in the species. Interestingly, the C−N bond length in the symmetrical species $(CH_3{-}NH{-}CH_3)^{\bullet+}$ is calculated to be 1.442 Å. This shows a resonance bond character existing in the radical ion $(CH_3{-}NH{-}CH_3)^{\bullet+}$. *Ab initio* MO calculations applying the HF procedure using various basis sets show that the $(CH_3{-}NH{-}CH_3)^{\bullet+}$ has lower total energy, as seen in Table 1. As the second-order Møller−Plesset perturbation is taken into account, the calculated results at MP2/6-31G** and MP2/6-31+G** levels show that the $(CH_3{-}NH_2{-}CH_2)^{\bullet+}$ is slightly more stable than the $(CH_3{-}NH{-}CH_3)^{\bullet+}$ by less than 3 kJ/mol.

For larger MMA cluster ions $(CH_3NH_2)_nH^+$ ($n \geq 3$), the above arrangement and fragmentation processes were not observed. This inhibition on the arrangement and fragmentation may result from the solvation effect of the cluster ion. Similar behaviors were also found in the large DMA and TMA cluster ion systems.

4.2.2. DMA Cluster Ions. The peak corresponding to the immonium ion $(CH_3{-}NH{=}CH_2)^+$ (mass 44) is clearly seen in Figure 1c. As mentioned above, this ion results from the 1,2-hydrogen elimination and the C=N formation in the protonated DMA monomer, $(CH_3{-}NH_2{-}CH_3)^+$. The commonly seen satellite peak at mass 42 can be assigned to the ions of the form $(CH_3{-}N{\equiv}CH)^+$ or $(CH_2{=}N{=}CH_2)^+$. Its appearance further indicates a 1,2-hydrogen elimination and the formation of a C≡N or a second C=N bond in $(CH_3{-}NH{=}CH_2)^+$. The calculated total energies of these two isomeric species using *ab initio* methods are listed in Table 1. The results predict that the $(CH_3{-}N{\equiv}CH)^+$ is more stable than the $(CH_2{=}N{=}CH_2)^+$ by about 70 kJ/mol using the MP2/6-31+G** calculations. The calculated results show that the C−N and C≡N bond lengths in the $(CH_3{-}N{\equiv}CH)^+$, are 1.447 and 1.158 Å, respectively, whereas the C=N bond length in the $(CH_2{=}N{=}CH_2)^+$ is 1.259 Å.

The peak at mass 30 in Figure 1c arises from the ion signals of $(NH_2{=}CH_2)^+$. This suggests that the rearrangement and

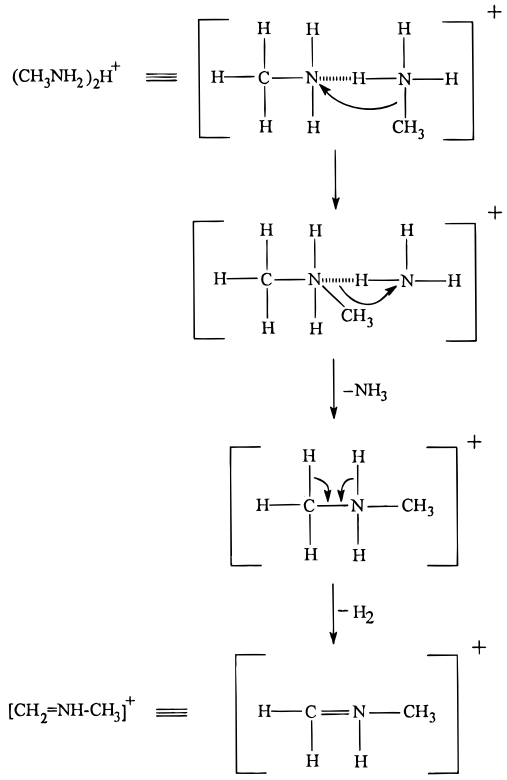

Figure 3. Possible fragmentation scheme for $(CH_3NH_2)_2H^+$ cluster ions.

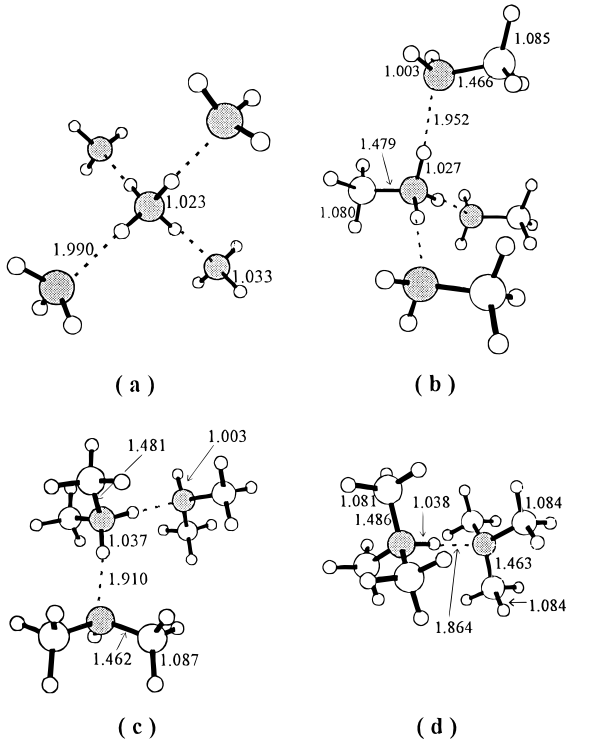

Figure 4. Fully optimized geometries of (a) $(NH_3)_5H^+$, (b) $(CH_3NH_2)_4H^+$, (c) $[(CH_3)_2NH]_3H^+$, and (d) $[(CH_3)_3N]_2H^+$ cluster ions at the HF/6-31G** level of calculations. The bond distances shown are in Å.

fragmentation processes in $(CH_3{-}NH_2{-}CH_3)^+$ involve the loss of a CH_4 molecule as well as the formation of C═N bond. The peak at mass 28 is assigned to $(NH{\equiv}CH)^+$ which is produced by losing a CH_2 radical from $(CH_3{-}N{\equiv}CH)^+$ or the 1,2-hydrogen elimination from $(NH_2{=}CH_2)^+$.

4.2.3. TMA Cluster Ions. The protonated TMA monomer has the form $[(CH_3)_3N]H^+$ (mass 60) which can undergo 1,2-hydrogen elimination resulting in the formation of a C═N bond. This process leads to the formation of $[(CH_3)_2N{=}CH_2]^+$ (mass 58) which may proceed with a rearrangement to lose a CH_2 species to form $(CH_3{-}NH{=}CH_2)^+$ (mass 44). Observation of a relatively small peak at mass 42 suggests that the $(CH_3{-}NH{=}CH_2)^+$ may also undergo 1,2-hydrogen elimination to form $(CH_3{-}N{\equiv}CH)^+$. This ionic species is commonly found in the mass spectra of ionized pyrrolidines and piperidines where the nitrogen is actually in the ring.[16] Our findings therefore indicate that intracluster fragmentation of ionized TMA clusters may involve the formation of intermediate species similar to ionized pyrrolidines and piperidines.

4.3. Cluster Ion Stability and Structure Implication. It has been shown that small neutral polymers ($n = 3{-}6$) including ammonia, MMA, DMA, and TMA clusters are expected to have cyclic structures.[21] However, the corresponding cluster ions may or may not have the same cyclic structures. For example, $(NH_3)_5H^+$ is believed to have a shell structure consisting of a central NH_4^+ ion core with four surrounding NH_3.[1−5] Similar stable structures have been proposed for many mixed hydrogen-bonded cluster ions.[22−27] As a general rule, stable hydrogen-bonded cluster ions are formed whenever all available hydrogen-bonding sites on the "central ion" are filled.

4.3.1. Optimized Geometries. Figure 4 depicts the fully optimized geometries of $(NH_3)_5H^+$, $(CH_3NH_2)_4H^+$, $[(CH_3)_2NH]_3H^+$, and $[(CH_3)_3N]_2H^+$ cluster ions at the HF/6-31G** level of calculation. The N−H bond length of the central NH_4^+ in $(NH_3)_5H^+$ is 1.023 Å which is slightly longer than the corresponding bond length of 1.012 Å for the bare ammonium ion. This results from the clustering interaction between the central NH_4^+ and the outer NH_3 molecule due to lone pair electrons on the nitrogen atom of the NH_3. The intracluster NH···N bond distance is calculated to be 1.990 Å. The ∠N−H···N is essentially linear, which indicates a strong hydrogen bonding between the central ion and the surrounding molecules. The zero dipole moment implies that the $(NH_3)_5H^+$ has a highly symmetrical geometry where all the hydrogen-bonding sites of the central NH_4^+ are occupied by the NH_3 molecules.[9]

In the case of $(CH_3NH_2)_4H^+$, the N−H bond length of the central $CH_3NH_3^+$ is 1.027 Å which is slightly longer than the corresponding 1.010 Å for the bare $CH_3NH_3^+$ ion. The C−N bond length is calculated to be 1.479 Å for the central ion $CH_3NH_3^+$ and 1.466 Å for the outer neutral CH_3NH_2. The equilibrium NH···N bond distance between the central $CH_3NH_3^+$ and the outer CH_3NH_2 is calculated to be 1.952 Å, which is less than that found in ammonia cluster ions, indicating that the interaction between the central ion and the outer molecules in $(CH_3NH_2)_4H^+$ is stronger than that in $(NH_3)_5H^+$.

The calculated N−H bond length of the central $(CH_3)_2NH_2^+$ in the $[(CH_3)_2NH]_3H^+$ and that of the central $(CH_3)_3NH^+$ in the $[(CH_3)_3N]_2H^+$ are all slightly longer than those in the corresponding bare ions, as seen in Figure 4. The NH···N intracluster bond distances in $[(CH_3)_2NH]_3H^+$ and $[(CH_3)_3N]_2H^+$ are predicted to be 1.909 and 1.864 Å. The C−N bond lengths in the $[(CH_3)_2NH]_3H^+$ and $(CH_3)_3NH^+$ are slightly shorter than those in the corresponding bare ions.

For the $(CH_3NH_2)_4H^+$, $[(CH_3)_2NH]_3H^+$, and $[(CH_3)_3N]_2H^+$ cluster ions, it is found that the C−N bond length in the central core ion is always longer than that in the outer neutral molecules. Since all ∠NH···N deviate from 180° by no more than 4°, the hydrogen-bonding character is expected to exist in these cluster ions. Furthermore, the extent of the longer N−H bond and the shorter NH···N clustering bond distance reveals the relative strength of the clustering interactions between the central ion and the surrounding neutral molecules. Our calculated results show that the strength of the clustering interaction is as follows,

$$(NH_3)_5H^+ < (CH_3NH_2)_4H^+ < [(CH_3)_2NH]_3H^+ < [(CH_3)_3N]_2H^+ \quad (8)$$

The proton affinities of ammonia, MMA, DMA, and TMA have been measured to be 853.5, 896, 923, and 942 kJ/mol, respectively.[19] Therefore, the interaction within these cluster ions seems to reflect the bonding nature of the constituent molecules. This trend is confirmed by the calculations of cluster ion stabilization energies presented in the following section.

4.3.2. Stabilization Energies. The calculated stabilization energy $\Delta E_{n-1,n}$ is defined as the follows

$$\Delta E_{n-1,n} = E(A_nH^+) - E(A_{n-1}H^+) - E(A) \quad (9)$$

where E is the calculated total energy of the species A (= NH_3, MMA, DMA, or TMA). Tables 2 and 3 display the calculated stabilization energies $\Delta E_{n-1,n}$ for the $(NH_3)_nH^+$, $(CH_3NH_2)_nH^+$, $[(CH_3)_2NH]_nH^+$, and $[(CH_3)_3N]_nH^+$. Although the calculations using 3-21G basis set overestimated the stabilization energy, the calculated values using the 3-21G basis set were found to be in qualitative agreement with the observed distribution of cluster ions.

As seen in Table 2, there is a drastic decrease from $\Delta E_{4,5}$ to $\Delta E_{5,6}$, indicating that the $(NH_3)_5H^+$ is particularly stable among the protonated ammonia cluster ions. This result is consistent with that reported in the literature.[28] Similar results were found for the MMA and TMA cluster ion systems, as shown in Table 3. Unfortunately, the total energy of $[(CH_3)_2NH)]_4H^+$ could not be obtained with our present computation facilities. Thus, it is concluded that the $(CH_3NH_2)_4H^+$, $[(CH_3)_2NH]_3H^+$, and $[(CH_3)_3N]_2H^+$ are also relatively stable among the corresponding cluster ions. This enhanced stability results from the complete filling of the hydrogen bonding sites on the "central ions".

The HF/6-31+G* calculations only slightly overestimate the proton affinities of ammonia, MMA, DMA, and TMA molecules by about 5%, as shown in Tables 2 and 3, which indicate that the inclusion of larger basis sets can give a more accurate prediction on the proton affinity. Since most of the calculated values are in reasonable agreement with the experimental ones, our *ab initio* calculations provide a reasonable estimation on the stabilization energies of several protonated MMA, DMA, and TMA cluster ions.

4.3.3. Charge Distributions. Calculations on the charge distribution was quite helpful in understanding the stability of cluster ions shown in Figure 4. On the basis of Mulliken[29] population analysis of the HF/6-31G** calculations, the central ions of the stable $(NH_3)_5H^+$, $(CH_3NH_2)_4H^+$, $[(CH_3)_2NH]_3H^+$, and $[(CH_3)_3N]_2H^+$ retain total positive charges of 0.80, 0.82, 0.86, and 0.92, respectively, whereas the total positive charges on the corresponding ligand NH_3, CH_3NH_2, $(CH_3)_2NH$, and $(CH_3)_3N$ are 0.05, 0.06, 0.07, and 0.08. Our observations on charge distributions of ammonia cluster ions are in very good agreement with those reported.[1,2] The trend in the charge distribution is also consistent with that of the stabilization energy and the intracluster bond distance as discussed previously.

5. Conclusion

The present study indicates that the observed major product ions resulting from prompt fragmentation following ionization are $(NH_3)_nH^+$ (n = 1−32), $(CH_3NH_2)_nH^+$ (n = 1−24), $[(CH_3)_2NH]_nH^+$ (n = 1−17), and $[(CH_3)_3N)_nH^+$ (n = 1−10). Based on the detected product ions and fragments, reasonable intracluster reactions, rearrangements and fragmentations were proposed. *Ab initio* MO calculations predict that the asymmetric $(CH_3-N\equiv CH)^+$ is more stable than its isomeric species $(CH_2=N=CH_2)^+$. Similarly, the asymmetric $(CH_3-NH_2-CH_2)^{\bullet+}$ was found to be slightly more stable than its symmetric isomer $(CH_3-NH-CH_3)^{\bullet+}$.

Anomalously large relative intensities observed for cluster ions $(NH_3)_5H^+$, $(CH_3NH_2)_4H^+$, $[(CH_3)_2NH]_3H^+$, and $[(CH_3)_3N]_2H^+$ were attributed to enhanced stability due to complete filling of hydrogen-bonding sites of the corresponding "central ions" NH_4^+, $CH_3NH_3^+$, $(CH_3)_2NH_2^+$, and $(CH_3)_3NH^+$. This argument is supported by *ab initio* calculations on the stabilization energies and the optimized geometries of these cluster ions.

Acknowledgment. We gratefully acknowledge the financial support from the National Science Council of the Republic of China (Grant No. NSC-85-0213-M-001-030).

References and Notes

(1) Deakyne, C. A. *J. Phys. Chem.* **1986**, *90*, 6625.
(2) Deakyne, C. A.; Meot-Ner, M.; Campbell, C. L.; Hughes, M. G.; Murphy, S. P. *J. Chem. Phys.* **1986**, *84*, 4958.
(3) Price, J. M.; Croton, M. W.; Lee, Y. T. *J. Chem. Phys.* **1989**, *91*, 2749.
(4) Lifshitz, C.; Louage, F. *J. Phys. Chem.* **1989**, *93*, 5633; *Int. J. Mass Spectrom. Ion Processes* **1990**, *101*, 101.
(5) Wei, S.; Tzeng, W. B.; Castleman Jr., A. W. *J. Chem. Phys.* **1990**, *92*, 332; **1990**, *93*, 2506.
(6) Booze, J. A.; Baer, T. *J. Chem. Phys.* **1992**, *96*, 5541.
(7) Desai, S. R.; Feigerle, C. S.; Miller, J. C. *J. Chem. Phys.* **1992**, *97*, 1793.
(8) Castleman Jr., A. W.; Tzeng, W. B.; Wei, S.; Morgan, S. *J. Chem. Soc., Faraday Trans.* **1990**, *86*, 2417.
(9) Hirao, K.; Fujikawa, T.; Konishi, H.; Yamabe, S. *Chem. Phys. Lett.* **1984**, *104*, 184.
(10) Bisling, P.; Rühl, E.; Brutschy, B.; Baumgärtel, H. *J. Phys. Chem.* **1987**, *91*, 4310.
(11) Brutschy, B.; Bisling, P.; Rühl, E.; Baumgärtel, H. *Z. Phys. D* **1987**, *5*, 217.
(12) Brutschy, B. *J. Phys. Chem.* **1990**, *94*, 8637.
(13) Tsai, W. C.; Yeh, W. H.; Tzeng, W. B. *J. Chin. Chem. Soc.* **1994**, *41*, 505.
(14) Wang, C. R. C.; Hsu, C. C.; Liu, W. Y.; Tsai, W. C.; Tzeng, W. B. *Rev. Sci. Instrum.* **1994**, *65*, 2776.
(15) *Gaussian 94*, Revision B.2; Frisch, M. J., Trucks, G. W., Schlegel, H. B., Gill, P. M. W., Johnson, B. G., Robb, M. A., Cheeseman, J. R., Keith, T., Petersson, G. A., Montgomery, J. A., Raghavachari, K., Al-Laham, M. A., Zakrzewski, V. G., Ortiz, J. V., Foresman, J. B., Cioslowski, J., Stefanov, B. B., Nanayakkara, A., Challacombe, M., Peng, C. Y., Ayala, P. Y., Chen, W., Wong, M. W., Andres, J. L., Replogle, E. S., Gomperts, R., Martin, R. L., Fox, D. J., Binkley, J. S., Defrees, D. J., Baker, J., Stewart, J. P., Head-Gordon, M., Gonzalez, C., Pople, J. A. Gaussian, Inc.: Pittsburgh, PA, 1995.
(16) Davis, R.; Frearson, M. *Mass Spectrometry*; John Wiley & Sons: Singapore, 1991; pp 324−330.
(17) Misaizu, F.; Houston, P. L.; Nishi, N. *J. Chem. Phys.* **1993**, *98*, 336.
(18) Lias, S. G.; Bartmess, J. E.; Liebman, J. F.; Holmes, J. L.; Levin, R. D.; Mallard, W. G. *J. Phys. Chem. Ref. Data* **1988**, *17*, Suppl. No. 1.
(19) Lias, S. G.; Liebman, J. F.; Levin, R. D. *J. Phys. Chem. Ref. Data* **1984**, *13*, 695.
(20) McMillen, D. R.; Golden, D. M. *Annu. Rev. Phys. Chem.* **1982**, *33*, 493.
(21) Odutola, J. A.; Viswanathan, R.; Dyke, T. R. *J. Am. Chem. Soc.* **1979**, *101*, 4787.
(22) Tzeng, W. B.; Wei, S.; Neyer, D. W.; Keesee, R. G.; Castleman Jr., A. W. *J. Am. Chem. Soc.* **1990**, *112*, 4097.
(23) Tzeng, W. B.; Wei, S.; Castleman Jr., A. W. *Chem. Phys. Lett.* **1990**, *166*, 343; *J. Phys. Chem.* **1991**, *95*, 5757.
(24) Wei, S.; Tzeng, W. B.; Castleman Jr., A. W. *Chem. Phys. Lett.* **1991**, *178*, 411; *J. Phys. Chem.* **1991**, *95*, 585; *Z. Phys. D* **1991**, *20*, 47.
(25) Wei, S.; Tzeng, W. B.; Keesee, R. G.; Castleman Jr., A. W. *J. Am. Chem. Soc.* **1991**, *113*, 1960.
(26) Herron, W. J.; Coolbaugh, M. T.; Vaidyanathan, G.; Peifer, W. R.; Garvey, J. F. *J. Am. Chem. Soc.* **1992**, *114*, 3684.
(27) Vaidyanathan, G.; Herron, W. J.; Garvey, J. F. *J. Phys. Chem.* **1993**, *97*, 7880.
(28) Keesee, R. G.; Castleman Jr., A. W. *J. Phys. Chem. Ref. Data* **1986**, *15*, 1011.
(29) Mulliken, R. S. *J. Chem. Phys.* **1955**, *23*, 1833.

JP961303B